ChemComm

COMMUNICATION

View Article Online
View Journal

Cite this: DOI: 10.1039/c4cc07444k

Received 21st September 2014,
Accepted 5th November 2014

DOI: 10.1039/c4cc07444k

www.rsc.org/chemcomm

Li_3VO_4 anchored graphene nanosheets for long-life and high-rate lithium-ion batteries†

Zelang Jian,[a] Mingbo Zheng,[b] Yanliang Liang,[a] Xiaoxue Zhang,[a] Saman Gheytani,[a] Yucheng Lan,[c] Yi Shi[b] and Yan Yao*[ad]

Li_3VO_4 nanoparticles embedded in graphene nanosheets (Li_3VO_4@GNS) were obtained using a sol–gel method. The composite presents excellent high-rate performance with a stable capacity of 133 mA h g^{-1} at 50 C and long-life performance with a capacity retention rate of 63.1% after 5000 cycles at 5 C.

Lithium-ion batteries (LIBs) have been widely used as power sources for portable electronics with potential applications in electric vehicles and large-scale energy storage devices because of their high energy density, high power density, and environmentally friendly features.[1] Graphite is commonly used as an anode material in most commercial LIBs. However, graphite reaches almost 0 V *vs.* Li^+/Li at the end of the discharge process,[2] a potential at which dendritic lithium could grow on the anode surface and lead to safety issues.[3] Spinel $Li_4Ti_5O_{12}$ has attracted wide attention as a promising anode material because of its minimal volume change and relatively high voltage during Li^+ insertion/extraction.[4] Although $Li_4Ti_5O_{12}$ shows good cyclability and high safety, it suffers from low capacity (175 mA h g^{-1}) and a relatively high intercalation potential at 1.54 V *vs.* Li^+/Li.[5] Recently, Li_3VO_4 has attracted increasing attention as a new anode material with suitable intercalation potential between 0.5 and 1 V *vs.* Li^+/Li. The potential is lower than that of $Li_4Ti_5O_{12}$ and higher than that of graphite. The theoretical capacity of Li_3VO_4 is 394 mA h g^{-1}, corresponding to a two-Li intercalation into the Li_3VO_4 structure. Furthermore, Li_3VO_4 has high ionic conductivity and has been studied as an ionic conductor for many years.[6,7] In contrast, the electronic conductivity of Li_3VO_4 is quite low and results in large resistance polarization and poor rate performance.[8] To improve the electrochemical performance, improving the electronic conductivity and reducing the particle size by growing inorganic nanoparticles on graphene has been proved to be an effective approach.[9,10]

In this study, we synthesized a Li_3VO_4@GNS (graphene nanosheets) nanocomposite as a novel anode material for LIBs, where Li_3VO_4 nanoparticles were embedded in GNS. This nanocomposite was obtained using a sol–gel method. Li_3VO_4 formed as fine crystals uniformly on GNS. The Li_3VO_4@GNS composite delivers excellent rate performance and cycling stability. Pristine Li_3VO_4 simply mixed with GNS was also prepared for comparison. Electrochemical impedance spectroscopy (EIS) was used for better understanding of the function of the composite.

Graphite oxide (GO) was synthesized from natural graphite powders using a modified Hummers method.[11] After thermal exfoliation of GO, GNS with a porous structure were obtained, which provide space to accommodate other materials.[12] Furthermore, the large amount of functional groups on the surface of GNS can supply adsorption sites for different ions.[12] Therefore, the Li_3VO_4@GNS composite can be prepared using the sol–gel method (the schematic illustration shown in Fig. 1). First, V_2O_5 powders were added into LiOH solution in stoichiometric quantities to form Li_3VO_4. After dissolving V_2O_5, a yellow solution was obtained with the formation of VO^{3-} ions [eqn (1)], after which GNS were added and stirred overnight to obtain

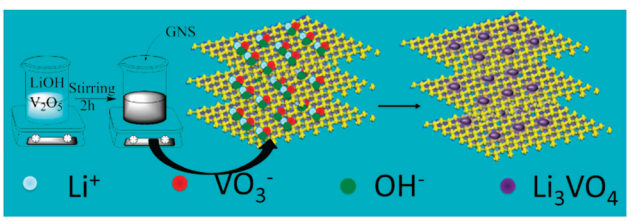

Fig. 1 Schematic illustration of the synthesis procedure of the Li_3VO_4@GNS composite.

[a] Department of Electrical and Computer Engineering and Materials Science and Engineering Program, University of Houston, Houston, TX 77204, USA. E-mail: yyao4@uh.edu
[b] Nanjing National Laboratory of Microstructures, School of Electronic Science and Engineering, Nanjing University, Nanjing 210093, China
[c] Department of Physics and Engineering Physics, Morgan State University, Baltimore, MD 21254, USA
[d] Texas Center for Superconductivity, University of Houston, Houston, TX 77204, USA

† Electronic supplementary information (ESI) available. See DOI: 10.1039/c4cc07444k

a black sediment. After calcination at 600 °C for 2 h, Li_3VO_4@GNS was obtained as the final product [eqn (2)].

$$2OH^- + V_2O_5 \rightarrow 2VO_3^- + H_2O \quad (1)$$

$$LiVO_3 + 2LiOH \rightarrow Li_3VO_4 + H_2O \quad (2)$$

More details of the experimental procedure are given in the ESI.†

Li_3VO_4 crystallizes in a cubic structure with a space group of $Pnm2_1$, where O ions form a hexagonal close-packed structure, while Li and V ions occupy 3/8 and 1/8 of tetrahedral interstitial sites, respectively (Fig. S1, ESI†). X-ray diffraction (XRD) patterns of pristine Li_3VO_4 and Li_3VO_4@GNS samples are shown in Fig. 2a. The diffraction peaks of both samples can be indexed into an orthorhombic Li_3VO_4 structure (JCPDS No. 38-1247). The LiO_6 and VO_6 tetrahedron are corner-shared to form a three dimensional structure. Estimation from the XRD peaks using the Scherrer equation revealed particle sizes of 53 nm and 34 nm for pristine Li_3VO_4 and Li_3VO_4@GNS, respectively. For the Li_3VO_4@GNS sample, a bump exists at around 25°, which could be assigned to the GNS. Raman spectroscopy is a powerful tool for characterizing graphitic structures. The peaks between 200 and 500 cm^{-1}, 750 and 1000 cm^{-1} are attributed to the Raman peaks of Li_3VO_4, which are in good agreement with the findings of a previous study.[8a] However, the intensity of these peaks for Li_3VO_4@GNS decreases sharply, indicating that Li_3VO_4 is well embedded inside the GNS and thus is hardly detectable by Raman spectroscopy. Two additional peaks located at 1345 cm^{-1} and 1595 cm^{-1} for the Li_3VO_4@GNS sample are attributed to the characteristic Raman peaks of the D-band and G-band of the graphitic material, respectively. The 26 wt% content of GNS in the Li_3VO_4@GNS composite was estimated by thermogravimetric analysis (Fig. S2, ESI†).

Scanning electron microscopy (SEM) and transmission electron microscopy (TEM) were used to further study the morphology of the two samples. Fig. 3a shows pristine Li_3VO_4 particles with two different sizes: bigger particles around 0.5–1 μm in size and smaller ones around 20–50 nm in size. Considering the XRD results shown in Fig. 2a, the sol–gel synthesis of Li_3VO_4 produces nanoparticles around 20–50 nm in size. During the calcination step, some of these nanoparticles aggregate to form large particles. Fig. 3b shows the interplanar spacing of the crystals of 0.37 nm, corresponding to the (101) plane. In the presence of GNS, the aggregation of Li_3VO_4 nanoparticles becomes more restricted with mostly small nanoparticles 10–30 nm in size

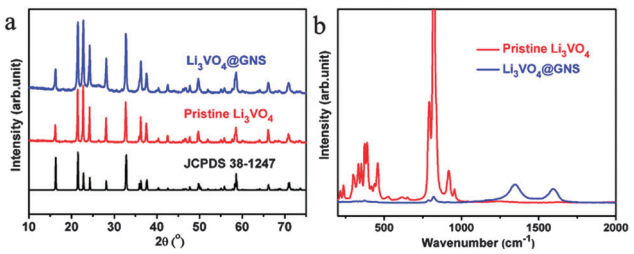

Fig. 2 (a) XRD patterns and (b) Raman spectra of the pristine Li_3VO_4 and the Li_3VO_4@GNS composite.

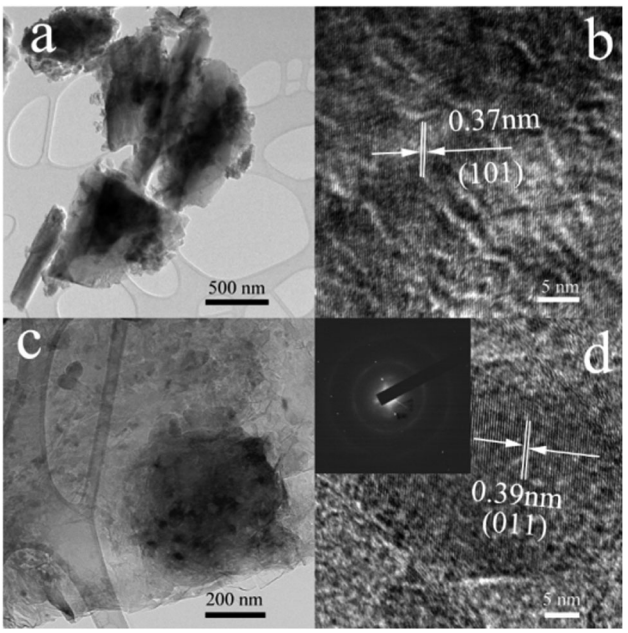

Fig. 3 (a) TEM image of pristine Li_3VO_4; (b) the HRTEM image of pristine Li_3VO_4; (c) the TEM image of the Li_3VO_4@GNS composite; (d) the HRTEM image of the Li_3VO_4@GNS composite; the inset shows the corresponding SAED pattern.

and less percentage of larger particles around 500 nm in size (Fig. S5, ESI†). The Li_3VO_4@GNS sample also shows a high degree of crystallinity. The crystalline interplanar spacing of 0.39 nm displayed in Fig. 3d corresponds to the (011) plane. The presence of the Li_3VO_4@GNS composite was further confirmed by the selected area electron diffraction (SAED) pattern (inset of Fig. 3d) owing to its characteristic diffraction rings and spots. The diffraction rings correspond to the (002) and (101) planes of GNS. The diffraction spots are indexed as crystals of Li_3VO_4, which are in good agreement with the XRD results.

The electrochemical performance of the Li_3VO_4@GNS composite was analysed in CR2032 coin cells. Fig. 4a shows the first three cycles of discharge/charge curves at a rate of 0.5 C (note that 0.5 C refers to two Li insertion into Li_3VO_4 per formula unit in 2 h). The initial discharge/charge capacity is 744/486 mA h g^{-1}, resulting in an irreversible capacity loss of 42%, which might be due to the formation of the solid electrolyte interface (SEI) film. The subsequent coulombic efficiency is improved over cycles; the coulombic efficiency for the second cycle can reach 94.6%. Cyclic voltammetry measurements were also performed and the corresponding first three cycles of the CV curves at a scan rate of 0.05 mV s^{-1} are shown in Fig. 4b. For the first cycle curve, two reduction peaks are found at 0.62 and 0.52 V, which shift to 0.86 and 0.53 V in the subsequent cycles, indicating a phase transformation during Li insertion. Only one broad oxidation bump at around 1.34 V can be observed in the first three cycles, indicating a similar lithium extraction mechanism.

We also investigated the rate performance of the Li_3VO_4@GNS composite. Stable capacities are observed at about 400, 350, 310, 256, 215, 175, and 133 mA h g^{-1} at rates of 0.5 C, 1 C, 2 C, 5 C, 10 C, 20 C and 50 C, respectively (Fig. 4c), ~90% of which is

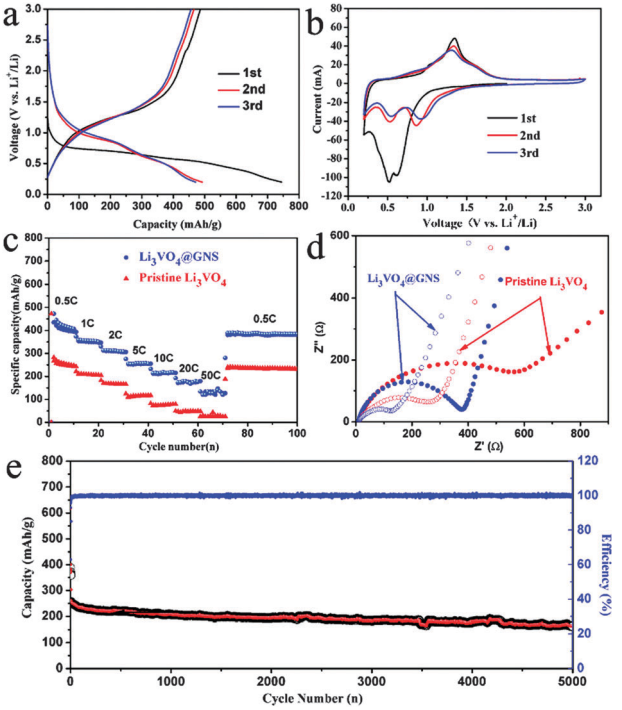

Fig. 4 (a) Galvanostatic discharge and charge profiles of the Li_3VO_4@GNS composite in the voltage range of 0.2–3 V *vs.* Li/Li^+ at a rate of 0.5 C; (b) the corresponding cyclic voltammetry curve of the Li_3VO_4@GNS composite at a scan rate of 0.05 mV s^{-1}; (c) discharge and charge capacities of pristine Li_3VO_4 and the Li_3VO_4@GNS composite at different C-rates, (d) Nyquist plots for pristine Li_3VO_4 and the Li_3VO_4@GNS composite before (solid) and after (hollow) the first cycle; (e) long-life performance of the Li_3VO_4@GNS composite at 5 C. All capacity calculations are based on the mass of Li_3VO_4.

due to Li_3VO_4 instead of GNS at all rates (Fig. S6, ESI†). Compared with the pristine Li_3VO_4 sample, simply mixed with 26 wt% of GNS as a conductive additive, the Li_3VO_4@GNS composite shows higher capacity, especially at high rates. For instance, the Li_3VO_4@GNS composite delivers a capacity of about 133 mA h g^{-1} at 50 C (8 mA h g^{-1} contributed from GNS), whereas the capacity of pristine Li_3VO_4 is almost zero. The significantly improved rate performance of this composite structure is attributed to the presence of small Li_3VO_4 particles and a close contact between Li_3VO_4 particles and GNS, which reduce the Li^+ ion diffusion distance and increase the electronic conductivity. Fig. 4d shows the EIS results of pristine Li_3VO_4 and the Li_3VO_4@GNS composite before and after discharge/charge. The Nyquist plots show a semicircle and a quasi-straight line (which represents the Warburg impedance, Z_W), which are associated with the charge transfer resistance (R_{ct}) and impedance of Li^+ diffusion in solid materials, respectively. Moreover, the values of R_{ct} for Li_3VO_4@GNS are obviously lower than those for pristine Li_3VO_4, indicating a better electronic contact of the Li_3VO_4@GNS electrode. The values of R_{ct} decrease after discharging/charging both electrodes, indicating a decrease in resistance after cycling. The long-life performance of the Li_3VO_4@GNS composite is shown in Fig. 4e. The capacity can be maintained at 163 mA h g^{-1} at a rate of 5 C after 5000 cycles, which is close to the theoretical capacity of $Li_4Ti_5O_{12}$. A capacity retention of about 63.1% and a coulombic efficiency close to 100% has been obtained after activation at 0.5 C for five cycles. The excellent long-life performance can be ascribed to the unique structure, in which Li_3VO_4 nanoparticles are well embedded inside GNS to form a structurally stable composite material (Fig. S7, ESI†).

In summary, we have designed a facile method to fabricate the Li_3VO_4@GNS composite, in which Li_3VO_4 nanoparticles (about 10–30 nm) are well embedded in GNS. This novel Li_3VO_4@GNS composite has been investigated as an anode material for LIBs. The composite presents excellent high-rate performance with a stable capacity of 133 mA h g^{-1} even at 50 C. After 5000 cycles at a rate of 5 C, its capacity is maintained at 163 mA h g^{-1}, which is 63.1% retention of the original reversible capacity. These results can be attributed to the formation of a conducting network of mixed Li^+ ions and electrons, as well as the protection provided by GNS in terms of reducing the side reaction between Li_3VO_4 and the electrolyte. These excellent properties make the Li_3VO_4@GNS composite structure a promising anode candidate for LIBs.

We acknowledge the support from the National Science Foundation (CMMI-1400261) and Robert A. Welch Professorship at TcSUH (E-0001).

Notes and references

1 (*a*) M. Armand and J.-M. Tarascon, *Nature*, 2008, **451**, 652; (*b*) C.-X. Zu and H. Li, *Energy Environ. Sci.*, 2011, **4**, 2614.
2 (*a*) T. Nagaura and K. Tozawa, *Prog. Batteries Sol. Cells*, 1990, **9**, 209; (*b*) K. Xu, *Chem. Rev.*, 2004, **104**, 4303.
3 G. Zheng, S. W. Lee, Z. Liang, H.-W. Lee, K. Yan, H. Yao, H. Wang, W. Li, S. Chu and Y. Cui, *Nat. Nanotechnol.*, 2014, **9**, 618.
4 (*a*) Z. Jian, L. Zhao, R. Wang, Y.-S. Hu, H. Li, W. Chen and L. Chen, *RSC Adv.*, 2012, **2**, 1751; (*b*) V. Etacheri, R. Marom, R. Elazari, G. Salitra and D. Aurbach, *Energy Environ. Sci.*, 2011, **4**, 3243.
5 L. El Ouatani, R. Dedryvere, C. Siret, P. Biensan and D. Gonbeau, *J. Electrochem. Soc.*, 2009, **156**, A468.
6 H. Li, X. Liu, T. Zhai, D. Li and H. Zhou, *Adv. Energy Mater.*, 2013, **3**, 428.
7 K. Gaur, A. Pathak and H. Lal, *J. Mater. Sci.*, 1988, **23**, 4257.
8 (*a*) Y. Shi, J.-Z. Wang, S.-L. Chou, D. Wexler, H.-J. Li, K. Ozawa, H.-K. Liu and Y.-P. Wu, *Nano Lett.*, 2013, **13**, 4715; (*b*) Y. Shi, J. Gao, H. D. Abruña, H. J. Li, H. K. Liu, D. Wexler, J. Z. Wang and Y. Wu, *Chem. – Eur. J.*, 2014, **20**, 5608; (*c*) Q. Li, J. Sheng, Q. Wei, Q. An, X. Wei, P. Zhang and L. Mai, *Nanoscale*, 2014, **6**, 11072.
9 (*a*) M. Zheng, D. Qiu, B. Zhao, L. Ma, X. Wang, Z. Lin, L. Pan, Y. Zheng and Y. Shi, *RSC Adv.*, 2013, **3**, 699; (*b*) L.-H. Hu, F.-Y. Wu, C.-T. Lin, A. N. Khlobystov and L.-J. Li, *Nat. Commun.*, 2013, **4**, 1687.
10 D. Wang, D. Choi, J. Li, Z. Yang, Z. Nie, R. Kou, D. Hu, C. Wang, L. V. Saraf and J. Zhang, *ACS Nano*, 2009, **3**, 907.
11 D. C. Marcano, D. V. Kosynkin, J. M. Berlin, A. Sinitskii, Z. Sun, A. Slesarev, L. B. Alemany, W. Lu and J. M. Tour, *ACS Nano*, 2010, **4**, 4806.
12 Z. Jian, B. Zhao, P. Liu, F. Li, M. Zheng, M. Chen, Y. Shi and H. Zhou, *Chem. Commun.*, 2014, **50**, 1215.